A ES
ISSN: 2096-3246
Volume 54, Issue 02, December, 2022
Special Issue

FOURIER PTYCHOGRAPHY IMAGINING TECHNIQUES: BASIC FOURIER PTYCHOGRAPHY, EXTENDED PTYCHOGRAPHY ITERATIVE ENGINE AND INCOHERENT IMAGING SYSTEM

Bhavye Singhal, Prayas Yadav
SGT University, Gurugram, Haryana, India

Pooja Singh
SGT University, Gurugram, Haryana, India
pooja_fps@sgtuniversity.org

Harendra Pal Singh
Babu Banarasi Das University, Lucknow (U.P.), India

Abstract
A developing method of computer microscopy called Fourier Ptychography can provide images of samples at a gigapixel resolution. An important tradeoff between a microscope's resolution and field of view is addressed by Fourier Ptychography without the need for any moving parts, merely requiring a reconstruction program and the attachment of an LED array to a standard digital microscope. This paper explains the ptychographic imaging, extended ptychograhic imaging, and incoherent imaging and hence discusses the result obtained from these methods on cameraman image.
Keywords: Field of view, Fourier Ptychography, Extended Fourier Ptychography, Incoherent Fourier Ptychography, Microscopy

1. Introduction

The resolution of an optical microscope is restricted by the numerical aperture of an objective lens. A large sample area is covered by objective lenses with a broad field of view (FOV), but the resolution is low. More sample features are captured by objective lenses with higher resolution, but only in a narrow area of the sample. This fundamental tradeoff primarily results from optical aberrations. Only a small portion of the image plane of a microscope can be optically corrected for aberrations. [1]. Lens space-bandwidth product (SBP) focuses on a small number of resolvable areas that a lens may carry from sample to plane. The degree of freedom that SBP can derive from an optical signal is known as SBP. In conventional microscope platforms, the SBP is frequently represented in megapixels. Few modern camera architectures have tried a solution within a microscope setup, but many try to overcome this physical barrier using collaboratively built optics and digital processing [2, 3].

1.1 Fourier Ptychography

An imaging method for high-bandwidth product imaging is called Fourier ptychography (FP) [4, 5]. An assembly of low-resolution (LR) images is taken that represent various Fourier sub-spectra of the sample. Wide field-of-view (FOV) and high-resolution (HR) images were obtained by merging sub-spectra collectively in Fourier space using a reconstruction technique. In Fourier Ptychographic

Microscopy (FPM), the incident light is regarded as a plane wave, and the LR images are obtained from the LEDs positioned at various locations under various incident angles. The measurements show various Fourier sub-spectra of the sample. The FPM's synthetic numerical aperture (NA) is about 0.5, and its field of view (FOV) is 120mm^2, which significantly increases the efficiency of a conventional microscope. FPM has been extensively used in 3D imaging [6, 7], fluorescence imaging [8, 9], mobile microscopy [10, 11], and high-speed in vitro imaging [12, 13] due to its simple setup. An array of LEDs and a standard microscope having low-NA objective lens make up a typical FP platform. The sample is sequentially illuminated using the LED array at various incident angles. For each illumination angle, FP records an image of the sample's LR intensity. Each image that results from the thin-sample assumption is specifically mapped to a particular passband of the spectrum of sample.

Afterwards, the FP algorithm improves an HR complex sample image by alternately compelling its amplitude to meet the collected LR images and its spectrum to satisfy the Fourier constraint. FP introduces angular diversity functions as opposed to translational diversity functions utilized in standard ptychography in order to retrieve the HR complex sample image [14].

1.2 Extended Ptychography Iterative Engine (ePIE):

Though PIE was a major success over the single intensity method it suffered reconstructions due to non-accurate values of probe position [7]. Knowing probe position and phase are very tedious and time-consuming task. So ePIE came into the picture. The update function for the probe is similar to the update function for the object of PIE.

If $P_k(r)$ is the estimated probe function for the k^{th} iteration, the probe update function will be:

$$P_{k+1}(r) = P_k(r) + b\frac{O_k^*(r + R^j)}{|O_k(r + R^j)|^2_{max}}(\psi^j_{c,k}(r) - \psi^j_k(r))$$

Thus now reconstruction problem greatly resolved for x-rays [8-14] and e-beams [15-18].

The conventional image is modelled in two steps as:

- Low pass filtering: The optical system here behaves as a low pass filter and here numerical aperture determines the cut-off frequency. Here optical system collects components in the spatial domain only an image is formed at the detector.
- Discrete sampling: The image sensor samples the light signal. Here one deciding factor for the pixel size of the image sensor is the Nyquist Criteria. These criteria must be satisfied.

PIE can be obtained using coherent imaging system as well as from coherent imaging system.

2. **Coherent Imaging System:**

Here spatially coherent light source is used for illumination. Here the phasor amplitudes change together at all spatial points. Therefore, a coherent imaging system has a linear complex amplitude:

$A_{output}(x, y) = h(x, y) \otimes A_{input}(x, y)$

where, $A_{input}(x, y)$=input complex amplitude

$A_{output}(x, y)$= output complex amplitude

$h(x, y)$= coherent point spread function in spatial domain

$\otimes$ = 2D convolution

We can transform the equation to frequency domain to obtain:

$$G_{coh\_output}(k_x, k_y) = H_{coh}(k_x, k_y)G_{coh\_input}(k_x, k_y)$$

where, $G_{coh\_input}(k_x, k_y)$ = Input Fourier spectrum of complex amplitude.

G_{coh_output} = Output Fourier spectrum of complex amplitude.

$H_{coh}(k_x, k_y)$ = Fourier transform of $h(x, y)$ or coherent transfer function

Condition for coherent illumination is that light must come from single point source.

First HR input object is created and a coherent imaging system is set up after which low pass filtering is done on the imaging system. This filter function is defined by a coherent transfer function. Here complex amplitude is transformed to the frequency domain and multiplied with a coherent transfer function. As a result, this spectrum is reversed. For the spatial domain, use the Fourier transform.

We note that coherent imaging is linear in complex amplitude and so the filtering process gives us complex amplitude and not intensity. So after getting the amplitude we usually convert it to intensity. Conventional image sensors are detecting the light intensity and so the phase information is completely lost and thus requires some algorithms to obtain the phase information [19-28] FP is such algorithm.

3. Incoherent Imaging System:

Unlike in a coherent imaging system, here the phasor amplitudes at different points do not vary together and instead vary differently. This illumination condition is called spatially incoherent. Here, the point spread function is a Mod Square of a coherent point spread function and the imaging system's intensity is linear:

$$I_{output}(x, y) = |h(x, y)|^2 \otimes I_{input}(x, y)$$

where, I_{input}: Input intensity image

I_{output}: Output intensity image

$|h(x, y)|^2$: Incoherent point spread function

Above equation can be transformed to Fourier domain to give:

$$G_{incoh\_output}(k_x, k_y) = H_{incoh}(k_x, k_y)G_{incoh\_input}(k_x, k_y)$$

where, G_{incoh_input} : input Fourier spectrum of intensity images

G_{incoh_output}: output Fourier spectrum of intensity images

H_{incoh}: Fourier transform of $|h(x, y)|^2$ known as incoherent transfer function

First we generate coherent transfer function and incoherent point spread function is obtained. This is transformed to frequency domain to give incoherent transfer function necessary for low pass filtering. Low pass filtered intensity output image is then obtained.

If we draw the comparison between the coherent and incoherent transfer functions then, we determine that the incoherent transfer function's cut-off frequency is double that of the coherent transfer function. However resolution is not determined by this, but depends on other factors where phase plays a key role.

4. Modelling Aberrations

Until now we have not considered effects of aberrations. In aberration free system resolution is determined by the numerical aperture. Here we introduce the optical aberration which is introduced

by a phase term in coherent transfer function as follows:

$\mathrm{CTF}(k_x, k_y) = \mathrm{circ}(\mathrm{NA}.\, k_o) e^{iW(k_x, ky)}$,

where,circ Function creates circular mask having radius of $\mathrm{NA}.\, k_o$

To incorporate aberrations in incoherent imaging system we convert coherent transfer function with aberrations to incoherent transfer function which is used in filtering to obtain output intensity image. More the aberrations lesser the resolution. We will later discuss the resolution and field of view parameters since we need both.

5. Simulation Results:

We verified different categories of Ptychography on different images. In the simulation, we assumed the wavelength of light is 0.63×10^{-6}m, the sampling size is 0.5×10^{-6} and the numerical aperture of the objective lens is 0.15. Root mean square error has been calculated. Computed result is shown below:

(a) Incoherent Ptychography on cameraman image:

Figure 1: Comparison of object recover from Inchorehent Ptychographing Imaging and Expected HR image

(b) Basic Ptychography iterative engine

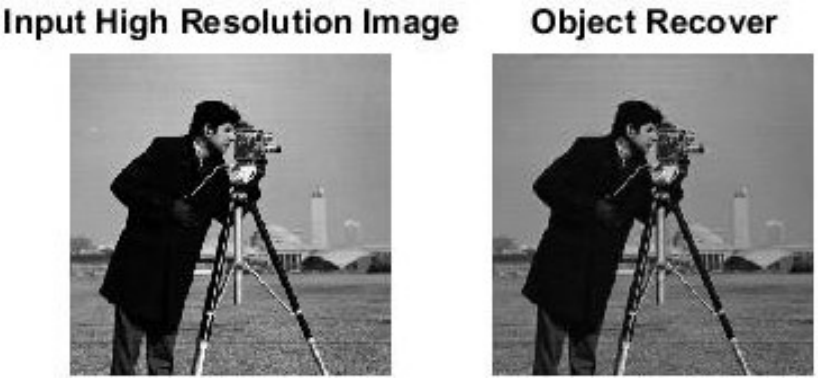

Figure 2: Comparison of object recover from Basic Ptychographing Imaging and Expected HR Image

(c) e - Ptychography Iterative Engine

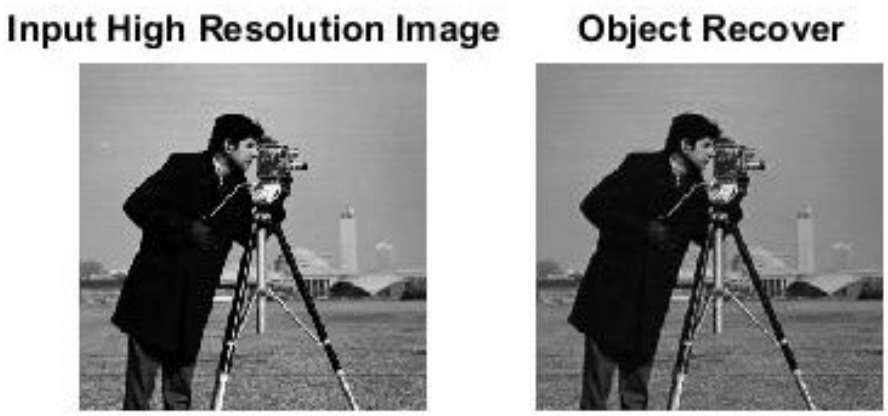

Figure 3: Comparison of object recover from e-Ptychographing Imaging and Expected HR Image

Table 1: Comparison of Root Mean Square Error for cameraman image using Incoherent Ptychography, Ptychographic Iterative Engine and e-Ptychographic Iterative Engine

Images	Incoherent Ptychography	Ptychographic Iterative Engine (PIE)	e-Ptychographic Iterative Engine (ePIE)
Cameraman	50.8667	202.4766	26.3759

6. Experimental Results:

The experiment is carried out using a conventional optical microscope and a low NA objective lens, consisting of a red-colored LED array (8×8) having 670 nm wavelength, an X-Y stage, and a microscopic camera. Low NA objective lenses can capture a wide field of view at the tradeoff of LR. The sample is illuminated from a variety of angles using an LED matrix. Through the low NA objective lens, FP captures an LR sample image at each illuminating angle. The array featured 3mm-diameter LEDs with a 4mm interLED gap. The source light in the microscope is replaced by red colored LED array connected to the base of the microscope. The sample holding stage height and hence the sample height can be adjusted using a knob and focus on the sample. The eyepiece of the microscope is replaced with a microscopic camera. This camera offers better noise performance. The microscopic camera is connected with Dell Laptop i5 by Future WinJoe interface, to capture the images.

As each of the 64 LEDs illuminated the sample in the LED matrix, a series of 64 LR images were taken. In the experiment, we considered the plant angiosperms as our sample. A microscopic camera is also used to take the LR images. The e-FPM technique uses these LR images as the initial raw data input to reconstruct HR images.

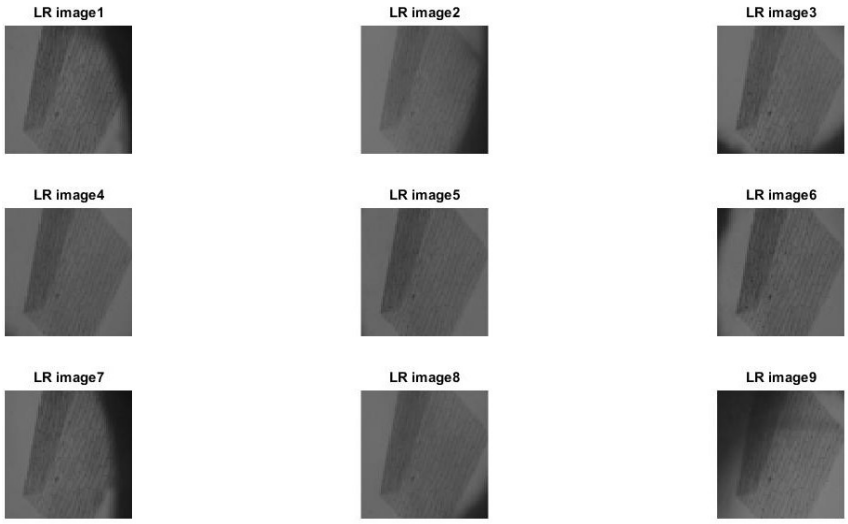

Figure 4: Captured LR images [64,64]

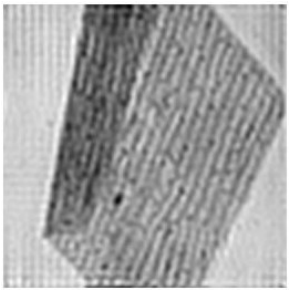

Figure 5: Recovered HR Image [256, 256]

7. Conclusions:

In this paper different categories of Fourier Ptychography Microscopy (FPM) algorithms such as incoherent FPM, basic FPM, and e-FPM on cameraman image are verified. With these observations, we calculated the root mean square between the expected HR image [256,256] and the HR image recovered with these FPM algorithms. For simulation, we considered the plant angiosperms image. Experimentally, we constructed an FP microscope to capture the LR images at different angles. Captured the 64 images of plant angiosperms and by using these LR images an HR image was constructed.

References:

1. Lohmann A, "Scaling laws for lens systems". Applied Optics; 28(23):4996–4998, 1989
2. Brady DJ, Gehm ME, Stack RA, Mark DL, Kittle DS, Golish DR, Vera EM, Feller SD, "Multiscale gigapixel photography", Nature. 2012; 486:386–389. [PubMed: 22722199]
3. Son HS, Johnson A, Stack R, Shaw JM, McLaughlin P, Marks DL, Brady DJ, Kim J. "Optomechanical design of a multiscale gigapixel digital camera." Applied Optics. 2013; 52(8):1541–1549.
4. G. Zheng, R. Horstmeyer, and C. Yang, "Wide-field, high-resolution Fourier

ptychographic microscopy," Nat. Photonics 7, 739–745 (2013).
5. X. Ou, R. Horstmeyer, C. Yang, and G. Zheng, "Quantitative phase imaging via Fourier ptychographic microscopy," Opt. Lett. 38, 4845–4848 (2013).
6. S. Dong, R. Horstmeyer, R. Shiradkar, K. Guo, X. Ou, Z. Bian, H. Xin, and G. Zheng, "Aperture-scanning Fourier ptychography for 3D refocusing and super -resolution macroscopic imaging," Opt. Express 22, 13586–13599 (2014).
7. L. Tian and L. Waller, "3D intensity and phase imaging from light field measurements in an LED array microscope," Optica 2, 104–111 (2015).
8. S. Dong, P. Nanda, R. Shiradkar, K. Guo, and G. Zheng, "High-resolution fluorescence imaging via patternilluminated Fourier ptychography," Opt. Express 22, 20856–20870 (2014).
9. J. Chung, J. Kim, X. Ou, R. Horstmeyer, and C. Yang, "Wide field-of-view fluorescence image deconvolution with aberration-estimation from Fourier ptychography," Biomed. Opt. Express 7, 352–368 (2016).
10. S. Dong, K. Guo, P. Nanda, R. Shiradkar, and G. Zheng, "FPscope: a field -portable high-resolution microscope using a cellphone lens," Biomed. Opt. Express 5, 3305–3310 (2014).
11. Z. F. Phillips, M. V. D'Ambrosio, L. Tian, J. J. Rulison, H. S. Patel, N. Sadras, A. V. Gande, N. A. Switz, D. A. Fletcher, and L. Waller, "Multi-contrast imaging and digital refocusing on a mobile microscope with a domed led array," PLoS ONE 10, e0124938 (2015).
12. L. Tian, Z. Liu, L.-H. Yeh, M. Chen, J. Zhong, and L. Waller, "Computational illumination for high-speed in vitro Fourier ptychographic microscopy," Optica 2, 904–911 (2015).
13. J. Chung, H. Lu, X. Ou, H. Zhou, and C. Yang, "Wide-field Fourier ptychographic microscopy using laser illumination source," arXiv:1602.02901 (2016).
14. M. Guizar-Sicairos and J. R. Fienup, "B Phase retrieval with transverse translation diversity: A nonlinear optimization approach", Opt. Exp., vol. 16, no. 10, pp. 7264–7278, May 2008.
15. Shehroz S. Khan and Amir Ahmad, "Cluster Centre Initialization Algorithm for K-means Cluster", In Pattern Recognition Letters, pp. 1293–1302, (2004).
16. Mahamed G.H. Omran, Andries P Engelbrecht and Ayed Salman, An "Overview of Clustering Methods", Intelligent Data Analysis (INTELL DATA ANAL), 2007.
17. Guoan Zheng, Roarke Horstmeyer and Changhuei Yang, "Wide-field, high -resolution Fourier ptychographic microscopy", Nat Photonics, 7(9): 739–745, 2013 September 1.
18. Roarke Horstmeyer, Xiaoze Ou1, Guoan Zheng, Phil Willems, and Changhuei Yang, "Digital pathology with Fourier ptychography", Comput Med Imaging Graph. 42: 38–43, 2015 June.

19. Liheng Bian, Guoan Zheng, Kaikai Guo, Jinli Suo, Changhuei Yang, Feng Chen, and Qionghai Dai, "Motion-corrected Fourier ptychography", Vol. 7, No. 11 BIOMEDICAL OPTICS EXPRESS 4543-53; 1 Nov 2016.
20. X. Ou, G. Zheng, and C. Yang, "Embedded pupil function recovery for Fourier ptychographic microscopy," Opt. Express 22, 4960–4972 (2014).
21. R. Horstmeyer, R. Y. Chen, X. Ou, B. Ames, J. A. Tropp, and C. Yang, "Solving ptychography with a convex relaxation," New J. Phys. 17, 053044 (2015).
22. L. Bian, J. Suo, G. Zheng, K. Guo, F. Chen, and Q. Dai, "Fourier ptychographic reconstruction using Wirtinger flow optimization," Opt. Express 23, 4856–4866 (2015).
23. L.-H. Yeh, J. Dong, J. Zhong, L. Tian, M. Chen, G. Tang, M. Soltanolkotabi, and L.Waller, "Experimental robustness of Fourier ptychography phase retrieval algorithms," Opt. Express 23, 33214–33240 (2015).
24. L. Bian, J. Suo, J. Chung, X. Ou, C. Yang, F. Chen, and Q. Dai, "Fourier ptychographic reconstruction using Poisson maximum likelihood and truncated Wirtinger gradient," Sci. Rep. 6, 27384 (2016).
25. D. Clausa, A. M. Maidena, F. Zhanga, A. Hursta, T. Edoa, F. Sweeneya, J. M. Rodenburga, H. Schluesenerb and M. J. Humphry, "Ptychography: A novel phase retrieval technique, advantages and its application", International Conference on Applications of Optics and Photonics, Proc. of SPIE Vol. 8001 800109-1-6, 1 Feb 2016
26. Armin Kappeler, Susho han Ghosh, Jason Holloway, Oliver Cossairt, Aggelos Katsaggelos, 'PTYCHNET : CNN based fourier Ptychography, IEEE International Conference on Image Processing (ICIP), 1712-16, 2017.
27. E. J. Candes, T. Strohmer, and V. Voroninski, "Phaselift: Exact and stable signal recovery from magnitude measurements via convex programming," Commun. Pure Appl. Math. 66, 1241–1274 (2013).
28. I. Waldspurger, A. d'Aspremont, and S. Mallat, "Phase recovery, maxcut and complex semidefinite programming," Math. Program. pp. 1–35 (2012).